



Micromechanics of soft materials using microfluidics

Yufan Xu, Hongjia Zhu, Yi Shen,* Alexander P. M. Guttenplan, Kadi L. Saar, Yuqian Lu, Daniele Vigolo, Laura S. Itzhaki, and Tuomas P. J. Knowles*

Impact statement

Soft and deformable materials exhibit a rich range of mechanical properties. Understanding the micromechanics of microgels is essential to explore strategies for sophisticated applications at the interface of soft materials and biology. Here, we developed a facile and cost-effective microfluidic assay to characterize the micromechanics of microgels. Taking advantage of parallelized design, we measured the shear modulus of protein microgels in a high-throughput and reproducible manner. The mechanical testing device in this present study is of great significance to the field of mechanics of materials at the microscale, with further potential applications in the understanding of the mechanical properties of soft objects such as organoids, artificial tissues, and other small and discrete clusters.

Micron-scale soft materials are finding a wide range of applications in bioengineering and molecular medicine, while also increasingly emerging as useful components for consumer products. The mechanical characterization of such microscale soft objects is conventionally performed with techniques such as atomic force microscopy or micropipette aspiration that measure the local properties of micron scale objects in a serial manner. To permit scalable characterization of the global mechanical properties of soft microscale objects, we developed and describe here a microfluidic platform that can be used for performing parallelized integrated measurements of the shear modulus of individual microscale particles. We demonstrate the effectiveness of this approach by characterizing the mechanical properties of multiple protein microgels in parallel, and show that the obtained values are in good agreement with conventional serial measurements. This platform allows parallelized *in situ* measurements of the mechanical properties of soft deformable micron-scale particles, and builds on scalable single-layer soft-photolithography fabrication, making the measurement system readily adaptable for a range of potential applications.

Introduction

Micron-scale soft materials are receiving increasing attention due to their diverse range of applications in areas such as drug delivery, regenerative medicine and the formation of microcapsules for food and household products.^{1–5} These particles include both artificial materials, such as hydrogels and microgels, and even intact living cells or their micron-scale subcellular compartments. It is frequently of interest

to determine the mechanical properties of such micron scale objects^{6–8} and a variety of methods has been described and developed to serve this purpose.^{4,9,10} In particular, atomic force microscopy^{11–13} and micropipette aspiration^{14,15} have been widely used for measuring the local properties of deformable objects. While these approaches permit understanding local mechanical properties and the responses at the surface of the particle, they do not readily provide

Yufan Xu, Hongjia Zhu, and Yi Shen have contributed equally to this study.

Yufan Xu, Centre for Misfolding Diseases, Yusuf Hamied Department of Chemistry, University of Cambridge, UK
 Hongjia Zhu, Centre for Misfolding Diseases, Yusuf Hamied Department of Chemistry, University of Cambridge, UK
 Yi Shen, Centre for Misfolding Diseases, Yusuf Hamied Department of Chemistry, University of Cambridge, UK; School of Chemical and Biomolecular Engineering, and The University of Sydney Nano Institute, The University of Sydney, Australia; yi.shen@sydney.edu.au
 Alexander P. M. Guttenplan, Centre for Misfolding Diseases, Yusuf Hamied Department of Chemistry, University of Cambridge, UK; Department of Pharmacology, University of Cambridge, UK;
 Kadi L. Saar, Centre for Misfolding Diseases, Yusuf Hamied Department of Chemistry, University of Cambridge, UK
 Yuqian Lu, Centre for Misfolding Diseases, Yusuf Hamied Department of Chemistry, University of Cambridge, UK
 Daniele Vigolo, The University of Sydney Nano Institute, and School of Biomedical Engineering, The University of Sydney, Australia; School of Chemical Engineering, University of Birmingham, UK;
 Laura S. Itzhaki, Department of Pharmacology, University of Cambridge, UK
 Tuomas P. J. Knowles, Centre for Misfolding Diseases, Yusuf Hamied Department of Chemistry, University of Cambridge, UK; Cavendish Laboratory, University of Cambridge, UK; tpjk2@cam.ac.uk

*Corresponding author

doi:10.1557/s43577-022-00279-5

information on the elastic response of the entire particle. Bulk rheological characterization approaches, by contrast, can be used to describe global mechanical properties of materials, but they require access to larger sample sizes that may be not compatible with micron-scale production approaches. Moreover, neither of these strategies allows direct *in situ* characterization of particles after formation. To open up the possibility of routinely characterizing the mechanical responses of individual micron-scale soft objects on a global scale, capillary micro-mechanics strategies have been proposed and demonstrated.¹⁶ These approaches involve trapping individual particles in tapered capillaries and observing the changes in their dimensions in response to applied forces. These changes simultaneously yield the compressive and shear modulus of the particles via classical continuum mechanics analysis.¹⁶ This is in contrast to flow-based approaches, such as deformation cytometry or interfacial tensiometry that enable a single property to be probed, and achieve this objective by requiring modeling of flow fields and the associated shear stresses in microfluidic channels for quantifying the mechanical parameters^{17,18} or require the calibration of the measurement setup with previously characterized materials.^{19,20} Capillary-based micromechanics based approaches have been demonstrated the ability to characterize both the properties of artificial microgels and the disease states of individual cells.^{16,21,22} The throughput of such approaches is, however, challenging to improve as to date typically only a single particle is analyzed at a given time.^{16,18}

To overcome these limitations and allow a number of individual micron-scale objects to be analyzed simultaneously, we designed and demonstrate here microfluidic poly(dimethylsiloxane)-based (PDMS-based) devices for parallel *in situ* measurements on the mechanical properties of individual micron-scale objects in an aqueous environment. The

devices were fabricated through a single step soft-lithography process and comprised a number of parallelized tapered channels across which the applied pressure differential could be adjusted to deform individual particles and extract their mechanical properties (Figure 1). We demonstrated the effectiveness of this strategy by characterizing the shear modulus of protein microgels as collagen substitute. The modular nature of microfluidics platform allows this strategy to be used for accessing the mechanical properties of micron-scale gels directly on chip in aqueous solutions, making their use attractive for applications that benefit from *in situ* analysis, such as the adjustment of operation parameters to produce particles with desired properties or the following of the progression of the polymerization and gelation process in real-time. The mechanical testing device can also find applications in the mapping of the mechanical properties of cell-laden microgels, artificial tissues, organoids, and biomolecular condensates.^{23–27}

Results

We used PDMS-based devices to probe the mechanical properties of protein microgel particles suspended in an aqueous solution. Prior to the measurement, microgels were fabricated from a single-T microdroplet device, and they were then demulsified from a continuous oil phase to a continuous aqueous phase (Figure 2a–b).²⁸ The resulted microgels were monodispersed with morphology (Figure 2b). In order to minimize the friction between the particles and the devices, all the channels were coated with PEG-silane to obtain a hydrophilic surface (Figure 2c, more details can be found in the “Materials and methods” section). This surface treatment of PDMS-based devices with PEG-silane complements the surface treatment of capillary-based devices with bovine serum albumin.¹⁶

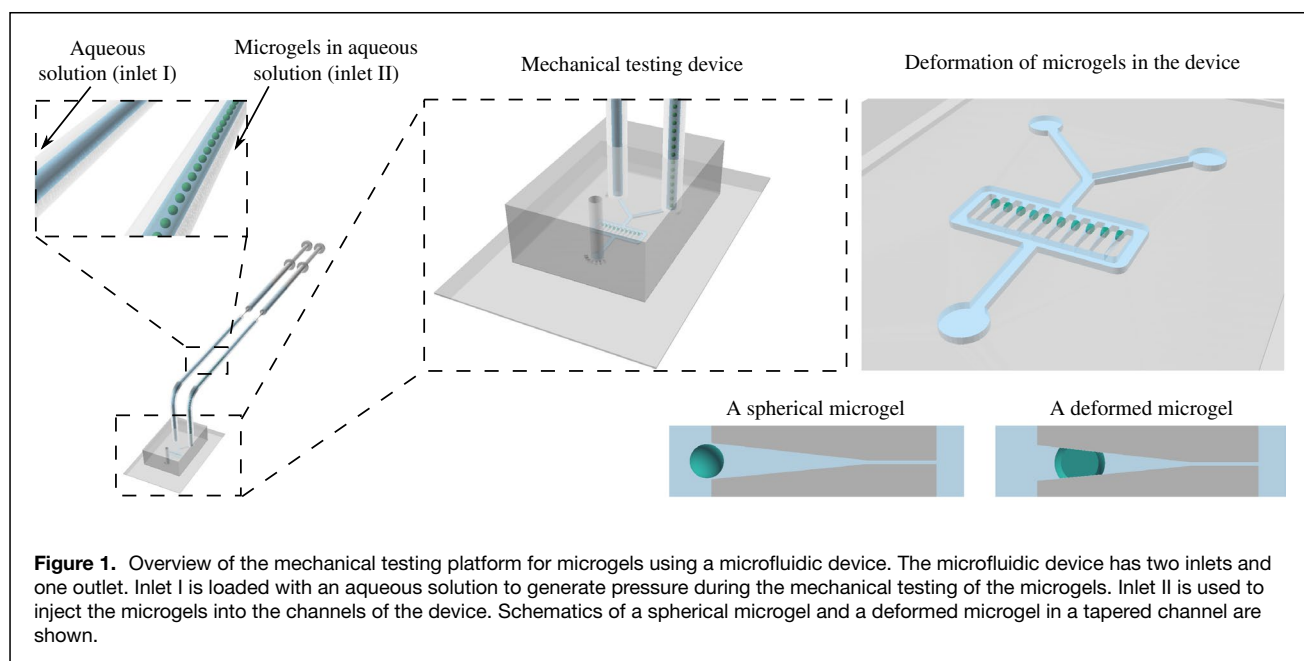


Figure 1. Overview of the mechanical testing platform for microgels using a microfluidic device. The microfluidic device has two inlets and one outlet. Inlet I is loaded with an aqueous solution to generate pressure during the mechanical testing of the microgels. Inlet II is used to inject the microgels into the channels of the device. Schematics of a spherical microgel and a deformed microgel in a tapered channel are shown.

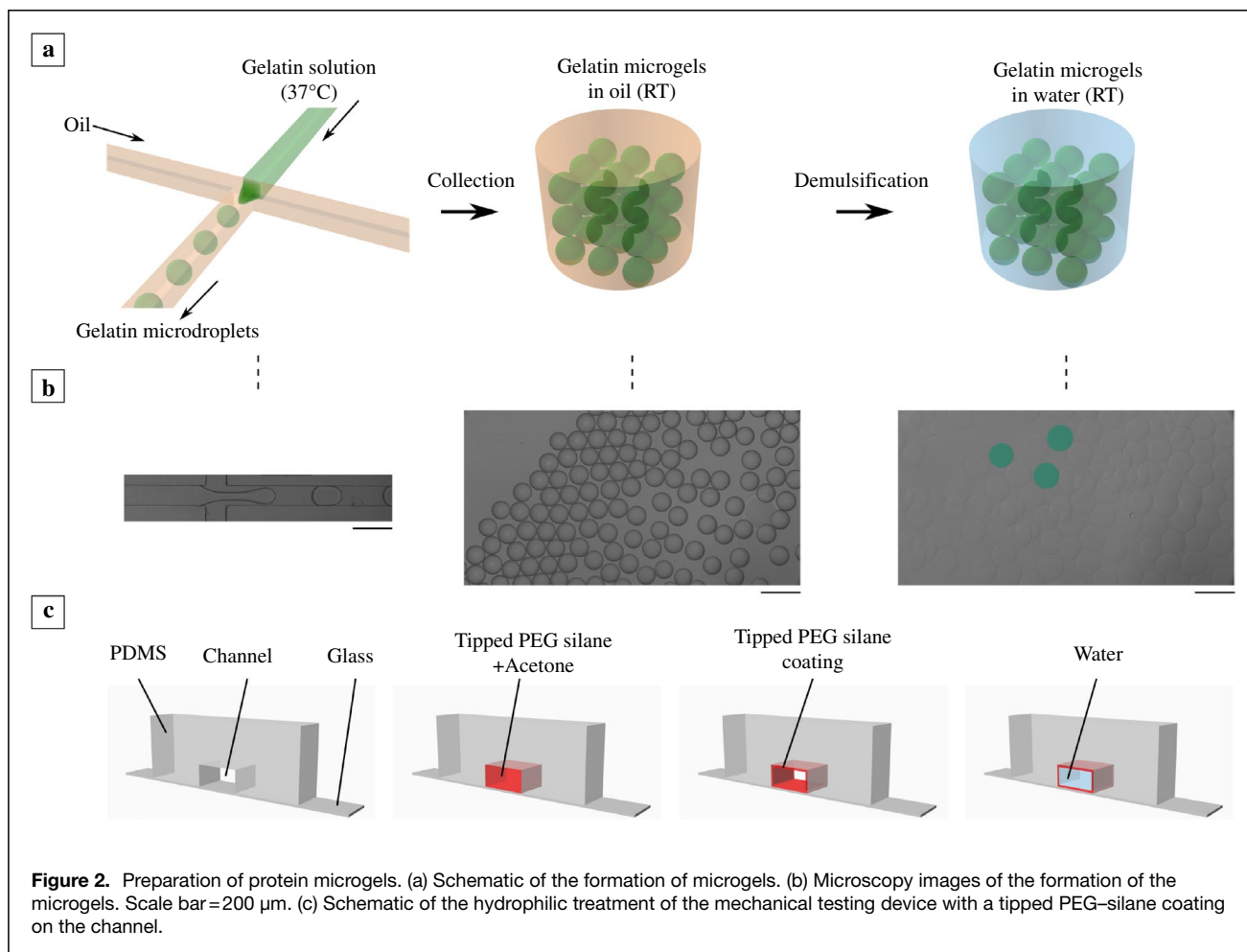


Figure 2. Preparation of protein microgels. (a) Schematic of the formation of microgels. (b) Microscopy images of the formation of the microgels. Scale bar = 200 μm . (c) Schematic of the hydrophilic treatment of the mechanical testing device with a tipped PEG-silane coating on the channel.

The microgel solution was introduced initially with a low flowrate. After the microgel particles were trapped in the tapered microfluidic channels, the flow of particles was turned off, and then the flowrate of the aqueous solution (Tris buffer) was set to increase from 0 to 2500 $\mu\text{L h}^{-1}$. The resulting deformation of the microgels in the tapered measurement channels in response to the applied pressures was recorded (Figure 3a, more details in Supplementary Material Figures S2, S3, S4; Movies S1, S2). We obtain the pressure drop across the tapered channels by running finite element simulation, which agreed well with estimates obtained from a dimensionality analysis (Figure 3b, detailed information can be found in Figure S1). The particles were seen to become more elongated when they moved further into the tapered channel with increasing flow both under 2D and 3D microscope imaging (Figure 3c–d). Furthermore, they moved back along the channel and recovered to the original shape when the flowrate was set to decrease from 2500 to 0 $\mu\text{L h}^{-1}$ (Figure 3e; Figures S2, S4; Movies S1, S2).

We were able to trap 10 microgels at once in the device (Figure 3h). Ten microgels could be readily trapped in the device within 90 s, indicating high trapping efficiency (Movie S4). After mechanical testing, the 10 microgels

can be released from the V-shaped channels by a slight mechanical vibration of microfluidic tubings (Movie S4); such release can allow the reuse of the device. From them, we performed image analysis and shear modulus estimation on three individual protein microgels trapped in three parallel measurement channels A–A' to C–C' (Figure S2c). The analysis of the microgels in their equilibrium position in the tapered channel allows us to estimate the shear moduli of the microgels. Indeed, based on a previous study,¹⁶ by plotting the relationship between the parameters $\frac{1}{2}(P_{\text{wall}} - \Delta P)$ and $(\epsilon_L - \epsilon_W)$, we estimate the shear modulus to be around 15 Pa for these microgels (Figure 3f, the detailed calculation can be found in the “Materials and methods” section). Physically cross-linked gelatin at lower concentration can be very soft. This value is in the same magnitude of the gelatin hydrogels at room temperature (RT) as previously reported (Table I).²⁹ In brief, the physically cross-linked gelatin demonstrated a lower shear modulus than some chemically cross-linked hydrogels (Table I). For the same particles, we were able to compress and decompress for three cycles (Figure S4). Similar results were obtained (Figure S3a–b), and the average shear moduli in

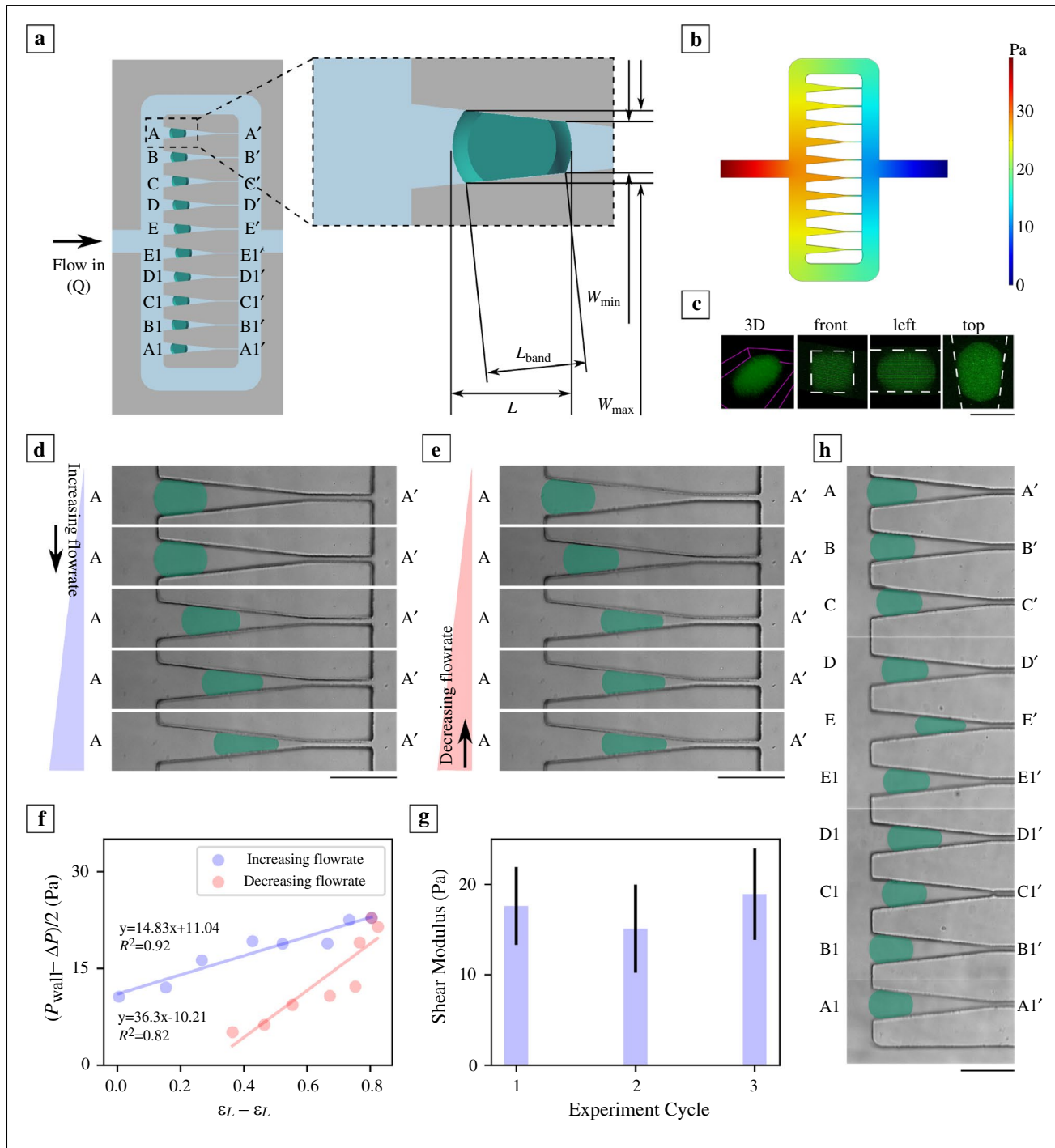


Figure 3. Mechanical testing of microgels in the microfluidic device. (a) Schematic of the microfluidic device trapping 10 microgels and the geometries to quantify their deformation. (b) Two-dimensional view of the finite element simulation (COMSOL) of the pressure drop in the microfluidic device (see Figure S1). (c) Three-dimensional confocal microscope imaging of a deformed microgel in the channel. Magenta lines indicate 3D. Dashed white lines indicate the microfluidic channels. (d, e) Deformation of a microgel at A-A' channel with increasing (d) and decreasing (e) flowrates. More is in Figure S2 (Movies S1, S2). (f) An example of data fitting (C-C', Figure S3). (g) Average shear modulus of microgels calculated during the 1st, 2nd, and 3rd increase of flowrate (Figure S3). (h) All 10 channels of the same device can trap microgels in one same experiment (Movies S3, S4). Scale bars = 100 μm (c) and 200 μm (d, e, h).


Table I. Comparison of the shear modulus obtained in this study to those in previously reported studies.

Materials	Shear Modulus (Pa)	Concentration (w/v) (%)	Material Form	More Information	References
Gelatin (this study)	ca. 15	5	Gelatin	Microfluidic device (25°C)	NA
Gelatin (previous studies)	10–820	5–15	Gelatin	Rheometer (20°C)	29
Alginate	203–3010	0.7–3	Alginate	Rheometer (25°C); M_w 418 kDa	30
	20–7000	6–8	Alginate + MAgel (varying cross-linking)	Rheometer (25°C)	31
Agarose	5570–18,660	0.9–2.7	Agarose	Ultrasound shear wave elastography	32
Poly(ethylene glycol) diacrylate (PEGDA)	100	10	PEGDA	Rheometer (37°C)	33
	26,000–220,000	10–20	PEGDA with or without agarose	Dynamic mechanical analyzer; M_w 2.0 kDa	34
	40,000–165,000	10–20	PEGDA with or without agarose	Dynamic mechanical analyzer; M_w 3.4 kDa	34
	22,000–110,000	10–20	PEGDA with or without agarose	Dynamic mechanical analyzer; M_w 6.0 kDa	34
Methacrylated gelatin (MAgel)	20–7000	7–10	Alginate + MAgel (varying cross-linking)	Rheometer (25°C)	31,33
Methacrylated chitosan (MAChi)	101	0.8	MAChi	Rheometer (37°C)	33
Methacrylated hyaluronic acid (MAHA)	10–110	0.5	MAHA (varying degree of methacrylation)	Rheometer (37°C)	33
Glycidyl methacrylate hyaluronic acid (GMHA)	16,000–73,000	2–10	GMHA (varying degree of methacrylation)	Texture analyzer	35

three cycles of experiments were concluded in Figure 3g. It was also noticed that, when the flowrates decreased, the microgels did not change the shape immediately (Figure 3f; Figures S2, S3, S4). We speculate that there was a delay between the decompression and the recovery of the deformation.

Discussion and conclusions

We have developed and described here a method for the mechanical characterization of soft micron-scale particles in aqueous solutions. Building on previously described capillary micromechanics method, the approach we have developed allowed multiple parallel measurements to be performed on individual micro- and mesoscale particles to obtain the shear moduli of each individual microgel. Being based on a microfluidic platform, the devices used for this analysis could be produced in a highly reproducible and scalable manner. Moreover, the measurement module could be combined with microgel formation processes to characterize the properties of the formed microgels *in situ* and, thus, could be used for performing kinetic analysis on the processes governing microgel formation, such as polymerization and aggregation reactions, or alternatively, for adjusting the parameters that control the formation of the microgels in real time in order to produce particles with desired properties. The microfluidic approach in this study also has the potential for the mechanical characterization of cells, tissues, and organ analogues at the microscale.

Materials and methods

Materials preparation

A homogeneous solution gelatin solution (w/v, 5%) was made by mixing gelatin powder (Fisher Scientific UK Ltd., Loughborough, UK) and Milli-Q water with a magnetic stirrer at 50°C. This gelatin solution was stored at 4°C and used within 2 weeks. An oil continuous solution was made by mixing fluorosurfactant (2%, w/w; RAN Biotechnologies, MA, US) with Fluorinert (FC-40; TM; Reg; Fluorochem, Hadfield, UK).

Microfluidic device fabrication

A single-T microfluidic device (i.e., droplet maker)²⁸ and a mechanical testing microfluidic device³⁶ with parallel tapered channels were fabricated by soft lithography techniques as previously reported.^{37,38} The single-T microfluidic device was treated hydrophobic.^{28,39–41} The mechanical testing microfluidic device was first treated hydrophilic for 500 s⁴² at power 8.0 in a plasma oven (Femto, Diener electronic GmbH+ Co. KG, Germany) and then the channels were rinsed with the mixture (v/v, 1/1) of acetone (Merck Life Science UK Limited, Dorset, UK) and tipped PEG silane (2-[methoxy(polyethyleneoxy)9-12propyl]trimethoxysilane, tech-90) (Gelest, Inc., Morrisville, USA) for 1 h; this acetone-based liquid was blown away by nitrogen before water was injected to clean and rinse the microfluidic channels. Acetone and tipped PEG silane were kept in a fumehood.

Table II. Geometrical data and the analysis of a microgel trapped in A–A' channel (e.g., increasing flowrate in the 1st cycle).

Flowrate ($\mu\text{L h}^{-1}$)	100	200	300	500	800	1000	1500	2000	2500
W_{\max} (μm)	111	110	109	98	87	85	76	72	65
W_{\min} (μm)	80	81	81	70	56	49	40	29	25
L_{band} (μm)	115	115	117	133	142	142	156	164	175
L (μm)	163	164	165	170	179	178	187	192	193
ΔP (Pa)	1.34901	2.69802	4.04703	6.74505	10.79208	13.4901	20.23515	26.9802	33.72526
$\epsilon_L - \epsilon_W$	NA	0.006135	0.0175055	0.1633636	0.3494684	0.3904539	0.5399094	0.6491183	0.7128449
$\frac{1}{2}(P_{\text{wall}} - \Delta P)$ (Pa)	2.65065	5.24139	7.60477	9.31951	11.48922	13.87632	15.05729	16.75852	15.12649

Microgel preparation

The gelatin solution and the oil continuous solution were injected into the single-T device, respectively,²⁸ and microdroplets were generated at 37°C, and then collected in an Eppendorf tube at RT for 10 min. To get microgels aqueous solution, the gelatin microdroplets were demulsified with 10% 1H,1H,2H,2H-perfluoro-1-octanol (Sigma-Aldrich Co. Ltd., MO, US) at RT or lower temperature.⁴³ 1H,1H,2H,2H-perfluoro-1-octanol was kept in a fumehood.

Probing the mechanics of microgels

To apply liquid pressure during the mechanical testing of microgels at RT, a 10 mL syringe (Hamilton) was used to inject an aqueous solution into the inlet I of the microfluidic device. A 1 mL syringe (Norm-Ject) was used to load microgels into the inlet II of the same device. A digital nEMESYS pump system (CETONI GmbH, Korbussen, Germany) was used to control the liquid pressure. After the well trapping of the microgels into the tapered channels of the microfluidic device, the syringe connecting inlet II was halted, while the syringe connecting inlet I continued working. The flowrate of the liquid in inlet I was increasingly set to be 100, 200, 300, 500, 800, 1000, 1500, 2000, and 2500 $\mu\text{L h}^{-1}$, and then was decreasingly set to be 2000, 1500, 1000, 800, 500, 300, 200, and 100 $\mu\text{L h}^{-1}$. Three replicates of this style of increasing and decreasing flowrates was done. Once each flowrate became stable, brightfield images of the deformation of microgels in the microfluidic device were taken by a CCD camera (CoolSNAP MYO, Photometrics, AZ, US) on a microscope (Observer. A1, Axio, Zeiss, Oberkochen, Germany).

Data analysis

As shown in Figures 1 and 3, the device has a main channel (width 200 μm , height 100 μm), and 10 parallel tapered channels (i.e., A–A', B–B', C–C', D–D', E–E', E1–E1', D1–D1', C1–C1', B1–B1', and A1–A1'). A pressure drop across tapered bridges was generated by flowing an aqueous solution with various flowrates mentioned above through the main channel. The pressure drop ΔP was calculated by the fluidic analogue of Ohm's Law,^{44,45}

$$\Delta P = RQ, \quad (1)$$

where R is the hydraulic resistance of the main channel that connects the two ends of a tapered channel, and Q is half of the flowrate of liquid from inlet I. For example, when a microgel was trapped in A–A' channel, ΔP is the applied pressure drop across the A–A' tapered bridges, and R is the hydraulic resistance in the main channel from position A to position A'.

For a rectangular cross section ($h < w$; h , channel height; w , channel width), the hydraulic resistance R was calculated based on the approximation,^{46,47}

$$R = \frac{12\eta L_m}{(1 - 0.63\frac{h}{w})wh^3}, \quad (2)$$

where L_m , h , and w are respectively the length, height, and width of the main channel in this study, and η is fluidic viscosity of the liquid in the main channel.

As shown in Figure 3a, under each flowrate of liquid from inlet I, W_{\max} , W_{\min} , L_{band} , and L of the deformed microgels were extracted from the images on ImageJ. P_{wall} is the pressure generated from PDMS walls (sidewall) of the tapered channels when the microgel was compressed, which can be derived as:¹⁶

$$P_{\text{wall}} = \frac{W_{\max}\Delta P}{2\sin\alpha L_{\text{band}}}, \quad (3)$$

where α is half of the tapered angle. P_{wall} and ΔP are in the horizontal plane (XY), as illustrated in Figure S5. The top and bottom walls of the tapered channels are parallel to each other, and thus the constrain in Z axis is constant throughout the channel; in the force equilibrium, the forces are canceled out.

The shear modulus of the microgel was then calculated based on a previous study,¹⁶

$$G = \frac{P_{\text{wall}} - \Delta P}{2(\epsilon_L - \epsilon_W)}, \quad (4)$$

where ϵ_L and ϵ_W are the strain of a microgel in the directions parallel and perpendicular to the channel length. Linear fitting was conducted on a scatter plot of $\frac{1}{2}(P_{\text{wall}} - \Delta P)$ versus $(\epsilon_L - \epsilon_W)$, and the slope is the value of shear modulus G .¹⁶

For example, Table II shows the data analysis of the deformation of a microgel trapped in A–A' channel (increasing flowrate of the 1st cycle), and shear modulus G of the



microgel can then be calculated (Figure 3a, f). ϵ_L is defined as $\frac{L}{L_0}$, where the L_0 is 163 μm at the initial flowrate of 100 $\mu\text{L h}^{-1}$, and corresponding L under each flowrate is demonstrated in Table II. ϵ_W is defined as $\frac{W}{W_0}$, where the W_0 is $\frac{W_{max0}+W_{min0}}{2} = \frac{111+80}{2}$ (μm) at the initial flowrate of 100 $\mu\text{L h}^{-1}$, and corresponding $W = \frac{W_{max}+W_{min}}{2}$ under each flowrate is calculated (Table II).

COMSOL simulation

COMSOL Multiphysics 5.2a was used to perform three dimensional simulations of the distribution of pressure in the aqueous single-phase within the mechanical testing device. A 3D laminar flow physics was used to determine the stationary pressure distribution within the microfluidic device. The required laminar inflow was imposed at the inlet while at the outlet the pressure, P , was fixed at $P=0$ Pa. The pressure drop at different tapered channels (A–A', B–B', C–C', D–D', and E–E') was then extracted from the distribution of pressure extracted from the middle plane ($z=50$ μm) and calculated as the difference between the wide-end and the narrow-end pressure of each tapered channel.

Acknowledgments

The research leading to these results has received funding from the Cambridge Trust (Y.X.), the Jardine Foundation (Y.X.), Trinity College Cambridge (Y.X.), China Scholarship Council (H.Z.), the Engineering and Physical Sciences Research Council (K.L.S.), the Schmidt Science Fellowship Program in partnership with the Rhodes Trust (K.L.S.), St John's College Cambridge (K.L.S.), EPSRC Cambridge NanoDTC (EP/037221/1; A.P.M.G.), the Newman Foundation (T.P.J.K.), the Wellcome Trust (T.P.J.K.), and the European Research Council under the European Union's Seventh Framework Programme (FP7/2007-2013) through the ERC Grant PhysProt (Agreement No. 337969; T.P.J.K.).

Author contributions

YX, HZ, and YS contributed equally to this project. YX, HZ, and YS performed the experiments. HZ analyzed the deformation data. APMG and KLS designed the microfluidic device concept, and YS, YL, and YX modified this design. DV performed the COMSOL simulation. YS and TPJK provided input into the experimental design and data analysis.

Code availability

Codes of analysis and plots can be provided by the authors upon reasonable requests.

Open Access

This article is licensed under a Creative Commons Attribution 4.0 International License, which permits use, sharing, adaptation, distribution and reproduction in any medium or format, as long as you give appropriate credit to the original author(s) and the source, provide a link to the Creative Commons

license, and indicate if changes were made. The images or other third party material in this article are included in the article's Creative Commons license, unless indicated otherwise in a credit line to the material. If material is not included in the article's Creative Commons license and your intended use is not permitted by statutory regulation or exceeds the permitted use, you will need to obtain permission directly from the copyright holder. To view a copy of this license, visit <http://creativecommons.org/licenses/by/4.0/>.

Supplementary Information

The online version contains supplementary material available at <https://doi.org/10.1557/s43577-022-00279-5>.

References

- N.A. Peppas, J.Z. Hilt, A. Khademhosseini, R. Langer, *Adv. Mater.* **18**, 1345 (2006)
- M. Malmsten, *Soft Matter* **2**, 760 (2006)
- A.S. Hoffman, *Adv. Drug Deliv. Rev.* **65**, 10 (2013)
- K.E. Kasza, A.C. Rowat, J. Liu, T.E. Angelini, C.P. Brangwynne, G.H. Koenderink, D.A. Weitz, *Curr. Opin. Cell Biol.* **19**, 101 (2007)
- B.G. Chung, K.-H. Lee, A. Khademhosseini, S.-H. Lee, *Lab Chip* **12**, 45 (2012)
- C. Duprat, H. Berthet, J.S. Wexler, O. Du Roure, A. Lindner, *Lab Chip* **15**, 244 (2015)
- M. Verhulsel, M. Vignes, S. Descroix, L. Malaquin, D.M. Vignjevic, J.-L. Viovy, *Biomaterials* **35**, 1816 (2014)
- J.K. Nunes, H. Constantin, H.A. Stone, *Soft Matter* **9**, 4227 (2013)
- P.A. Pullarkat, P.A. Fernández, A. Ott, *Phys. Rep.* **449**, 29 (2007)
- W.W. Ahmed, É. Fodor, T. Betz, *Biochim. Biophys. Acta Mol. Cell Res.* **1853**, 3083 (2015)
- T.R. Matzelle, G. Geuskens, N. Kruse, *Macromolecules* **36**, 2926 (2003)
- C. Rotsch, M. Radmacher, *Biophys. J.* **78**, 520 (2000)
- J. Wiedemair, M.J. Serpe, J. Kim, J.-F. Masson, L.A. Lyon, B. Mizaikoff, C. Kranz, *Langmuir* **23**, 130 (2007)
- R. Kwok, E. Evans, *Biophys. J.* **35**, 637 (1981)
- F. Guilak, J.R. Tedrow, R. Burgkart, *Biochem. Biophys. Res. Commun.* **269**, 781 (2000)
- H.M. Wyss, T. Franke, E. Mele, D.A. Weitz, *Soft Matter* **6**, 4550 (2010)
- A. Mietke, O. Otto, S. Girardo, P. Rosendahl, A. Taubenberger, S. Goffier, E. Ulbricht, S. Aland, J. Guck, E. Fischer-Friedrich, *Biophys. J.* **109**, 2023 (2015)
- O. Otto, P. Rosendahl, A. Mietke, S. Goffier, C. Herold, D. Klaue, S. Girardo, S. Pagliara, A. Ekpenyong, A. Jacobi, *Nat. Methods* **12**, 199 (2015)
- Q. Brosseau, J. Vrignon, J.-C. Baret, *Soft Matter* **10**, 3066 (2014)
- L. Kong, K.L. Saar, R. Jacquat, L. Hong, A. Levin, H. Gang, R. Ye, B. Mu, T.P.J. Knowles, *Interface Focus* **7**, 20170013 (2017)
- H.M. Wyss, J.M. Henderson, F.J. Byfield, L.A. Bruggeman, Y. Ding, C. Huang, J.H. Suh, T. Franke, E. Mele, M.R. Pollak, *Am. J. Physiol. Cell Physiol.* **300**, C397 (2011)
- A. Ravetto, H.M. Wyss, P.D. Anderson, J.M.J. den Toonder, C.V.C. Bouten, *PLoS ONE* **9**, e92814 (2014)
- G. Rossi, A. Manfrin, M.P. Lutolf, *Nat. Rev. Genet.* **19**, 671 (2018)
- T. Kamperman, S. Henke, A. van den Berg, S.R. Shin, A. Tamayol, A. Khademhosseini, M. Karperien, J. Leijten, *Adv. Healthc. Mater.* **6**, 1600913 (2017)
- I.A. Nyrkova, A.N. Semenov, A. Aggeli, N. Boden, *Eur. Phys. J. B* **17**, 481 (2000)
- Y. Shen, F.S. Ruggeri, D. Vigolo, A. Kamada, S. Qamar, A. Levin, C. Iserman, S. Alberti, P.S. George-Hyslop, T.P.J. Knowles, *Nat. Nanotechnol.* **15**, 841 (2020)
- L. Jawerth, E. Fischer-Friedrich, S. Saha, J. Wang, T. Franzmann, X. Zhang, J. Sachweh, M. Ruer, M. Ijavi, S. Saha, J. Mahamid, A.A. Hyman, F. Jülicher, *Science* **370**, 1317 (2020)
- Y. Xu, R.P.B. Jacquat, Y. Shen, D. Vigolo, D. Morse, S. Zhang, T.P.J. Knowles, *Small* **16**, 2000432 (2020)
- H. Kumagai, T. Fujii, T. Inukai, T. Yano, *Biosci. Biotechnol. Biochem.* **57**, 532 (1993)
- E.R. West, M. Xu, T.K. Woodruff, L.D. Shea, *Biomaterials* **28**, 4439 (2007)
- R. Seyedmahmoud, B. Çelebi-Saltik, N. Barros, R. Nasiri, E. Banton, A. Shamloo, N. Ashammakhi, M.R. Dokmeci, S. Ahadian, *Micromachines* **10**, 679 (2019)
- S. Sadeghi, D.H. Cortes, *J. Mech. Behav. Biomed. Mater.* **102**, 103502 (2020)
- D. Kim, B.-H. Cha, J. Ahn, Y. Arai, B. Choi, S.-H. Lee, *Adv. Funct. Mater.* **31**, 2007041 (2021)
- D.A. Rennerfeldt, A.N. Renth, Z. Talata, S.H. Gehrke, M.S. Detamore, *Biomaterials* **34**, 8241 (2013)
- S.A. Bencherif, A. Srinivasan, F. Horkay, J.O. Hollinger, K. Matyjaszewski, N.R. Washburn, *Biomaterials* **29**, 1739 (2008)
- A.P.M. Gутtenplan, Thesis, University of Cambridge (2018)



37. D.C. Duffy, J.C. McDonald, O.J.A. Schueller, G.M. Whitesides, *Anal. Chem.* **70**, 4974 (1998)
38. J.C. McDonald, D.C. Duffy, J.R. Anderson, D.T. Chiu, H. Wu, O.J.A. Schueller, G.M. Whitesides, *Electrophoresis* **21**, 27 (2000)
39. W.E. Arter, R. Qi, N.A. Erkamp, G. Krainer, K. Didi, T.J. Welsh, J. Acker, J. Nixon-Abell, S. Qamar, Y. Xu, J. Guillén-Boixet, T.M. Franzmann, D. Kuster, A.A. Hyman, A. Borodavka, P. St George-Hyslop, S. Alberti, T.P.J. Knowles, *bioRxiv* (2020). <https://doi.org/10.1101/2020.06.04.132308>
40. Y. Xu, R. Qi, H. Zhu, B. Li, Y. Shen, G. Krainer, D. Klenerman, T.P.J. Knowles, *Adv. Mater.* **33**, 2008670 (2021)
41. Y. Shen, A. Levin, A. Kamada, Z. Toprakcioglu, M. Rodriguez-Garcia, Y. Xu, T.P.J. Knowles, *ACS Nano* **15**, 5819 (2021)
42. Y. Zhang, T.W. Herling, S. Kreida, Q.A.E. Peter, T. Kartanas, S. Törnroth-Horsefield, S. Linse, T.P.J. Knowles, *Lab Chip* **20**, 3230 (2020)
43. Y. Xu, Y. Shen, T.C.T. Michaels, K.N. Baumann, D. Vigolo, Q. Peter, Y. Lu, K.L. Saar, D. Vella, H. Zhu, B. Li, H. Yang, A.P.M. Guttenplan, M. Rodriguez-Garcia, D. Klenerman, T.P.J. Knowles, *Adv. Mater. Interfaces* **8**, 2101071 (2021)
44. H.S. Damiri, H.K. Bardaweel, *Lab Chip* **15**, 4187 (2015)
45. D. Kim, N.C. Chesler, D.J. Beebe, *Lab Chip* **6**, 639 (2006)
46. H. Bruus, *Theoretical Microfluidics* (Oxford University Press, Oxford, 2008)
47. N.A. Mortensen, F. Okkels, H. Bruus, *Phys. Rev. E* **71**, 57301 (2005) □